Chapter V. Dust in fusion plasmas.

The fact that dust is present in the plasma of magnetic fusion devices is known for a long time (e.g. [1], [2], [3]). Already Ohkawa [1] had argued that dust particles can be an important source of impurity in fusion plasmas and can significantly degrade the performance of fusion plasmas. Later, experimental data confirmed that in some cases, the appearance of dust particles in fusion plasmas can even result in termination of the plasma discharge (e.g. see Fig. V.1 and Refs [4], [5]).

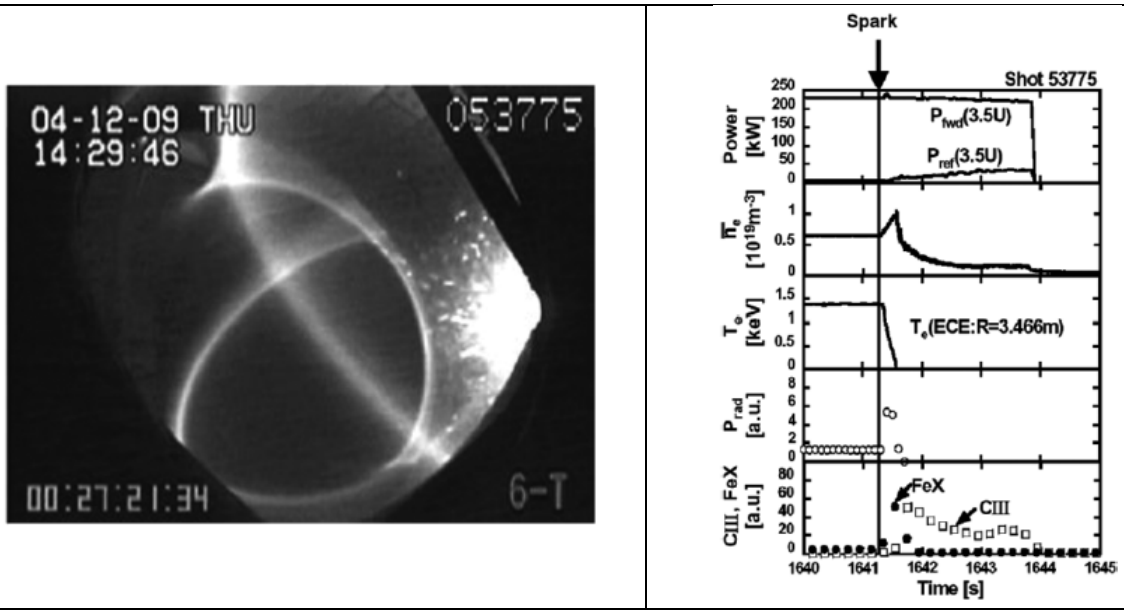

Fig. V.1 Spontaneous ejection ("spark) of dust particles from the first wall terminates a long pulse discharge in the LHD stellarator. The "spark" event observed with CCD camera (left) and time evolution of the plasma parameters (right). Reproduced with permission from [6], © Elseiver 2007.

The interest to the study of dust-related phenomena in fusion devices was boosted by the ITER project (see Refs. [7], [8], [9]). The main initial concern of the ITER staff was related to safety issues associated with the chemical activity, tritium retention and radioactivity of the dust [10] and the dust impact on the in-vessel plasma-facing diagnostics (e.g. mirrors) [11].

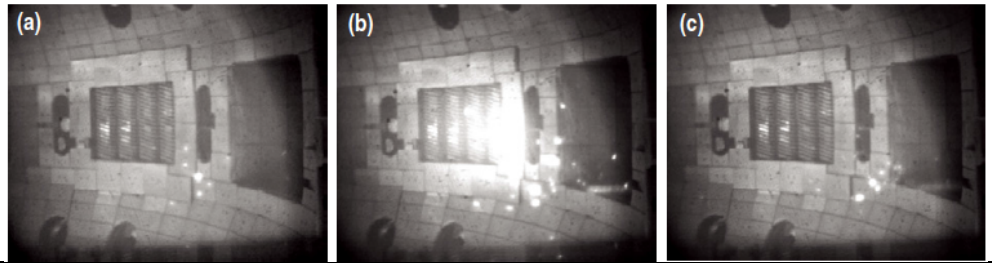

Fig. V.2. Dust observed by a fast camera in the DIII-D tokamak in front of the neutral beam injection (NBI) port 1 ms before (a), during (b) and 2 ms after (c) an NBI pulse. Reproduced with permission from [12], © IAEA 2009.

As of today, large amount of experimental data available on i) *in situ* dust observations with Thompson scattering diagnostics and fast cameras, which give information on the dust size distribution and the dynamics of dust motion (see Fig. V.2) through the plasma in fusion devices and ii) *post mortem* analysis of the shape (see Fig. V.3) and material composition of the dust particles collected in fusion devices (e.g. see [7], [13], [12], [14] [15], [16], [17], [18] and the references therein).

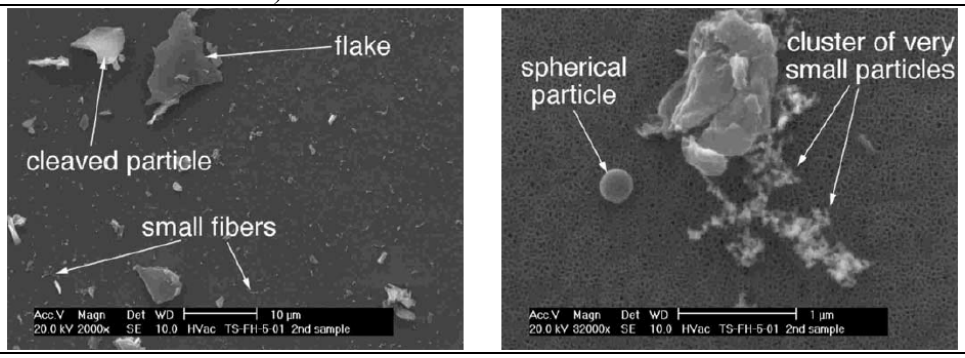

Fig. V.3. Dust particles of different shapes and sizes collected from fusion devices. Reproduced with permission from [19], © Elseiver 2002.

In this chapter, we will consider basic processes, related to a dust grain immersed into fusion plasma, which include grain charging, the forces acting on the grain and the grain dynamics. We review main dust-related experimental observations related to the dust parameters, constituency, and dynamics in fusion plasma, dust mobilization from the surfaces of the plasma-facing components, and compare some experimental data with the results of numerical simulations.

We also present an assessment of the impact of dust on ITER plasma performance and discuss the gaps in our understanding of dust physics in magnetic fusion devices.

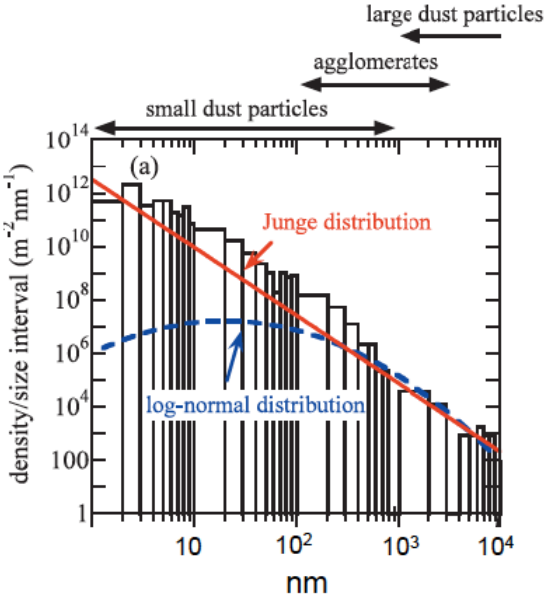

Fig. V.4. Size distribution of the dust particles found in LHD. Reproduced with permission from [20], © JSPF 2009.

V.1. Experimental study of dust in magnetic fusion devices.

V.1.1 Dust particle density, size distribution, and composition in fusion devices.

The size of the dust particles found in fusion devices is ranging from nano-meters (e.g. see Fig. V.4) to few hundred μm in the Alcator C-Mod tokamak [16]. Usually, the median diameter of a dust grain found in fusion devices is in the range of 1-10 μm [15]. The size distribution is often estimated from the dust collected from fusion devices during the ventilation events. But the result can depend on both the collection method and counting. For example,

counting with an optical microscope gives a log-normal distribution of dust particles [19], whereas counting with scanning (SEM) and transmission (TEM) electron microscopes reveals the presence of a large amount of sub-micron particles [21], [20]. As a result, the size distribution of dust particles of small diameters in the LHD device appears to be far from the log-normal distribution and close to the power-law distribution, $F_{dust}(\ell_d) \sim (\ell_d)^{-\alpha}$ (where ℓ_d is the characteristic size of the grain) with $\alpha \approx 2.5$ (see Fig. V.4).

However, dust mobilization from the plasma-facing components with subsequent penetration of the dust particles into the plasma volume depends on many circumstances (e.g. the initial location of the dust grains, the plasma parameters, etc.) [39], [17]. Therefore, the size distribution of dust collected from fusion devices during ventilation events can be different from that present in the plasma during discharges.

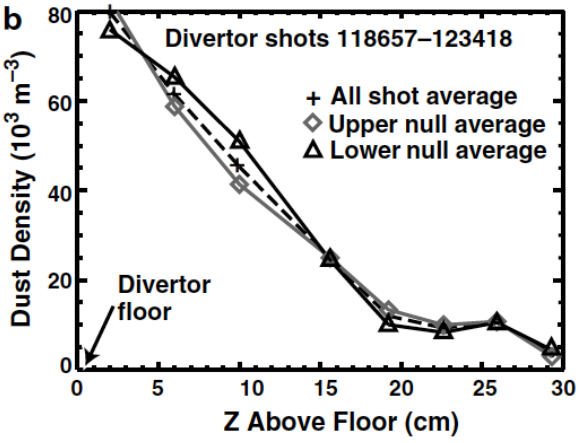

Fig. V.5. Dust particle density in low divertor of DIII-D. Reproduced with permission from [13], © Elseiver 2007.

Important information about the size and spatial distribution of the dust grains in the plasma of magnetic fusion devices can be obtained with laser scattering by utilizing the non-shifted (Rayleigh) channel of the Thomson scattering diagnostics used for the measurements of electron density and temperature. The first systematic studies of dust with laser scattering had been performed on the DIII-D tokamak [22], [13] and later laser scattering was used for dust detection in FTU [23] and JET [24]. The distribution of dust particle density found with laser scattering in low divertor of DIII-D is shown in Fig. V.5. Initial results on the size distribution of the dust grains, inferred from the laser scattering data using the Rayleigh theory of light scattering by particles [22], were reconsidered in [25] on the basis of the more correct Mie theory. In addition, in [25] dust grain ablation under intense laser radiation was taken into account. It was found that the size distribution function of the dust grains with radii in the range 0.01-10 μm (having averaged radius ~200 nm) in the DIII-D plasma can be described by the power-law distribution with $\alpha \approx 2.6 - 2.7$.

However, we should notice that larger grains can not be identified by laser scattering diagnostic due to the saturation of the measured reflected signal. We also note that similar power-law size distributions of the dust collected from LHD and measured in DIII-D plasma can be just a coincidence.

Observations of dust with the laser scattering technique show that the dust particle density at the edge of a magnetic fusion device depends strongly on the operational mode of the device. For example, in H-mode having rather violent MHD events such as ELMs (Edge Localized Modes), dust particle density in the SOL is few times higher than that in the "quiet" L-mode, Fig. V.6. In Fig. V.7 one can see the relaxation of the dust density just after an ELM burst (the solid line is the exponential fit with the characteristic half-time ~60 ms). An increase of the number of dust particles (dust mobilization events) in ELMy H-mode is also detected with "video diagnostic" (based on observations with fast cameras) developed

in the AUG tokamak [17]. However, one should take into account that fast cameras can only see relatively large dust grains (e.g. according to the assessment of Ref. [26], confirmed by the experimental data [27], for the case of carbon dust, the fast cameras can only see the grains with size $\gtrsim 1\,\mu m$).

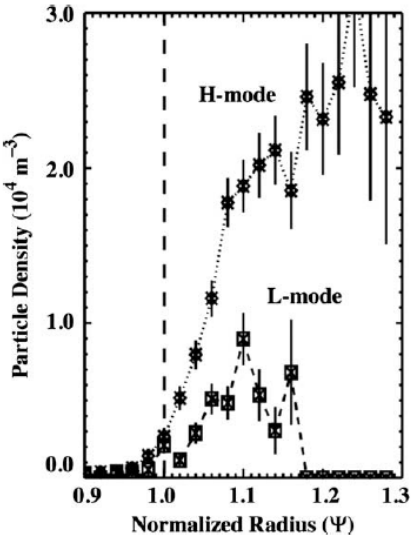

Fig. V.6. Dust density in the upper SOL of DIII-D for H- and L- confinement modes. Reproduced with permission from [28], © Elseiver 2009.

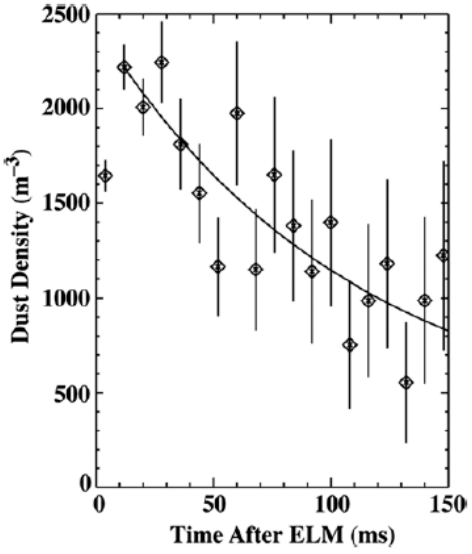

Fig. V.7. Time evolution of dust density after an ELM burst in DIII-D. Reproduced with permission from [28], © Elseiver 2009.

Experimental data demonstrate that density of the dust particles can depend not only on the power of auxiliary plasma heating (for example, an increase of neutral beam heating of DIII-D plasma from 2 MW to 13 MW increases the dust occurrence rate by a factor ten [13]) but also on the type of the auxiliary heating (e.g. with the electron- and ion- cyclotron waves, neutral beam injection, etc.) [17].

However, all available experimental data show that the largest amount of dust particles inside the vacuum chamber is observed after disruptions (see [15] and the references therein). For example, in the FTU tokamak, the dust particle density after a disruption can reach 10^7 m^{-3}, whereas, before the disruption, the laser scattering diagnostic detects no dust particles [23]. Moreover, the amount of dust remains higher than the average value during few shots after a disruption, Fig. V.8.

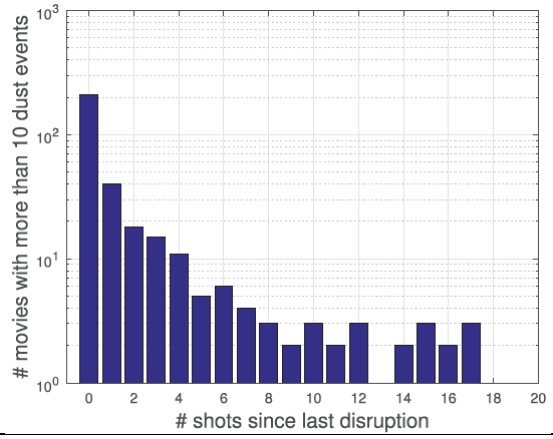

Fig. V.8. Effective number of dust particles in a discharge as a function of the number of discharges elapsed since a disruption. Reproduced with permission from [17], © IAEA 2017.

Although many elements contribute to the composition of the dust particles, the dominant one corresponds to the material of the plasma-facing and structural components used in current magnetic fusion devices, such

as carbon, tungsten, molybdenum, beryllium, lithium, etc. with the contribution from the material used for first wall conditioning (e.g. boron) (see Fig. V.9), as well as from hydrogen isotopes and impurities used for enhancing the radiation loss from the edge plasma (e.g. nitrogen) (see Refs. [29], [30] [16], [31] and the references therein). Some of the dust particles are agglomerations that have inclusions of very different materials (see Fig. V.10). We will see later that the dynamics of such agglomerated particles in fusion plasma can have very peculiar features.

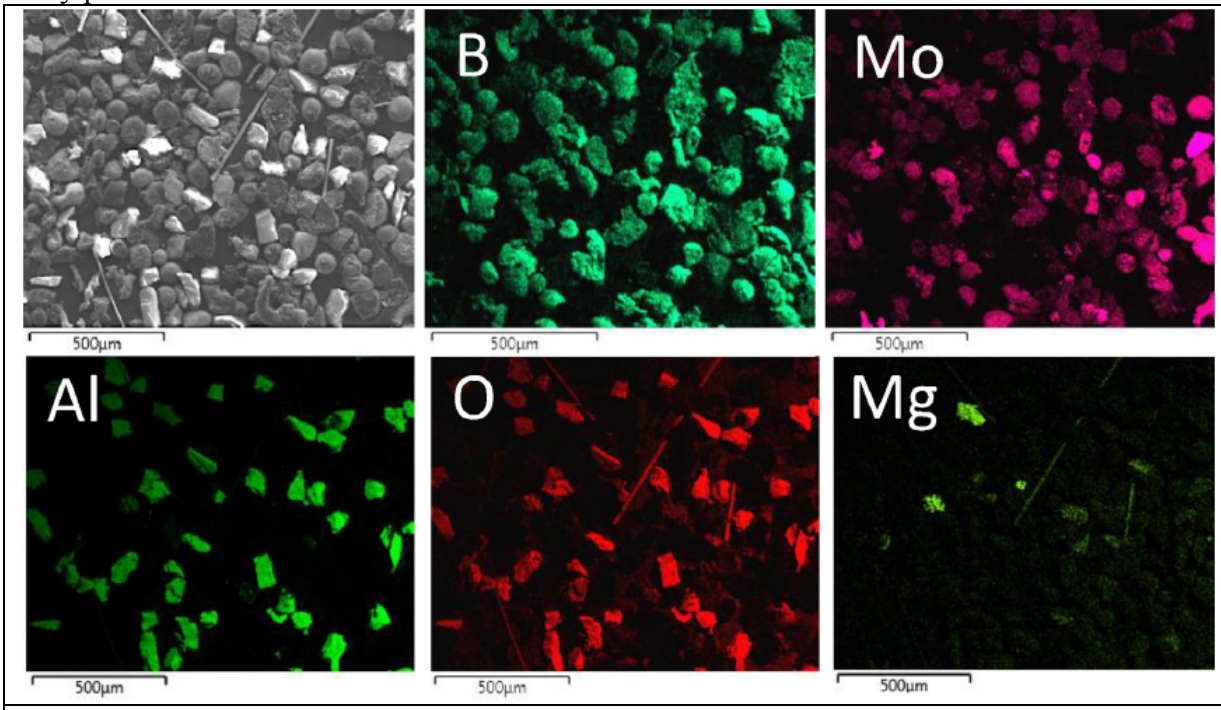

Fig. V.9. SEM image of dust particles (with a size range of 50-100 μm) collected from Alcator C-Mod. The energy-dispersive X-ray spectroscopy (EDX) mapping provides the composition of the dust grains. Reproduced with permission from [16], © Elseiver 2017.

Analysis of the dust particles collected in the major fusion devices [9], [32], [33], [34], [29], [35], [30] [16], [31] suggests that the main source of dust in the current magnetic fusion devices comes from melting of the edges of the metal tiles, arching, and exfoliation of co-deposited layers which, depending on the particular device, can consist of carbon, beryllium, boron, etc. with significant presence of hydrogen isotopes and some impurities.

V.1.2 Mobilization of dust particles from plasma-facing components.

Although postmortem analysis shows a significant amount of dust particles on the plasma-facing components virtually in all magnetic fusion devices, it is obvious that not all the dust ends up in the plasma at once. The mobilization of the dust

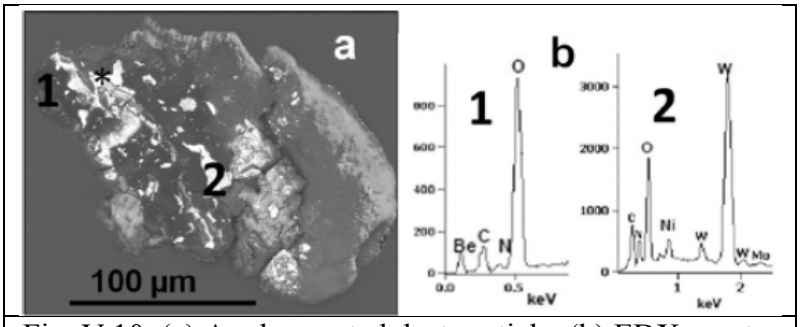

Fig. V.10. (a) Agglomerated dust particle, (b) EDX spectra from regions 1 and 2. Reproduced with permission from [31], © Elseiver 2017.

particles from the plasma-facing components is complex and is still the topic of ongoing research. Different mechanisms can be responsible for dust mobilization from the plasma-facing components: the plasma-induced drag force and dust collisions with the PFC surface [36], [37], [38], [39] (see Fig. V.11), splashes from molten metal targets [40], [41], [42], [43] (see Fig. V.12), thermal stresses resulting in cracking of the PFC material [44], [45] (in particular, of co-deposited layers having loose thermal contact with the bulk), etc.

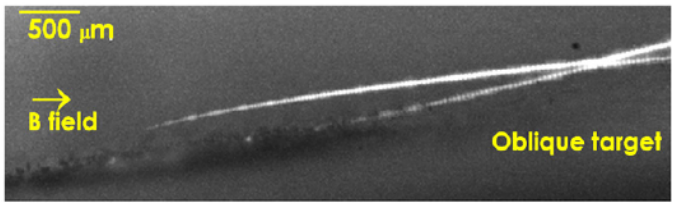

Fig. V.11. The trajectory of tungsten dust grain (observed with a fast camera) mobilized from the oblique polished plate in the Pilot-PSI device (the second image corresponds to the reflected light). Reproduced with permission from [46], © IAEA 2015.

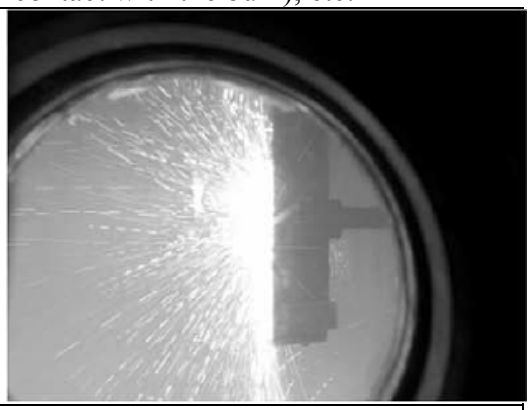

Fig. V.12. Photo of droplets ejected from a tungsten target melted under the exposure in the plasma accelerator QSPA-T. Reproduced with permission from [41], © Elseiver 2009.

V.1.3 Dust particle dynamics in fusion devices, experimental data.

The dynamics of dust particles in fusion devices is mainly studied with fast cameras. This is because the dust grains in fusion plasmas are heated up to high temperature and can start to ablate. As a result, we have two different radiation sources that can be captured by fast cameras: i) thermal radiation of the grain itself and ii) radiation from the ablation cloud related to the excitation of the ablated atoms by the ambient plasma electrons. Contributions of these two sources depend on both the dust material and the parameters of the ambient plasma (strictly speaking, the time history of the dust grain trajectory can also be important). However, the specifications of the fast camera can also matter.

Thorough analysis [26] of carbon dust observations in the DIII-D tokamak [38], [27] shows that for the DIII-D plasmas, thermal radiation of carbon dust particles only dominates in the far SOL, whereas radiation from the ablation cloud prevails in the relatively hotter and denser plasma close to the separatrix where the grain ablation rate is high. Although this analysis was performed for the carbon dust, the latter conclusion has robust physics arguments and seems to be very generic.

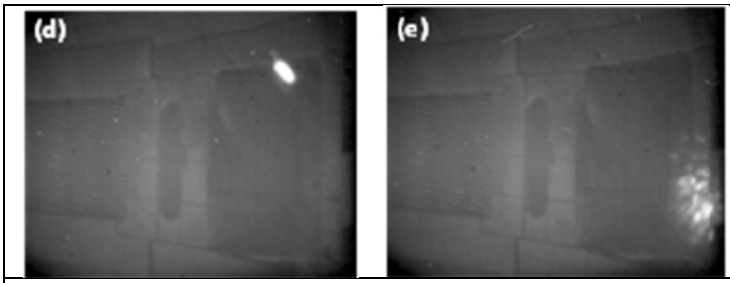

Fig. V.13. Fast (~500 m/s) dust particle moves toward the wall in DIII-D tokamak (left) and disintegrates after collision (right). Reproduced with permission from [47], © IOP Publishing 2008.

As of today, there are many photos and movies from virtually all major magnetic fusion devices [48], [6], [38], [49], [47] [27], [14] [50], [4], [51], [17], [52] showing dust traces in the plasma volume and, sometimes, collisions of dust particles with the PFCs (see Fig. V.13). Some movies are recorded with few different cameras, which allows determining both the dust speed and the 3D dust particle trajectory (e.g. see [49], [53]). These data can be used, in particular, for benchmarking the codes developed to study dust-related phenomena in fusion devices.

The results obtained with fast cameras show that the dust particles can acquire the speed ~ few hundred meters per second (e.g. [49], [38], [53]) and they move largely in the toroidal direction (e.g. see Fig. V.14). This is in agreement with the assessment made in [36], [37], where it was shown that the plasma drag force if one of the major forces exerted on a dust grain in fusion plasmas. Since the plasma in the inner and outer divertors flows in different toroidal directions, one can expect [37] that the toroidal components of the dust velocities in the inner and outer divertors should be opposite, which was indeed observed in the experiments (see Refs. [49], [12]). However, in [54] it was shown that toroidal plasma rotation can also be important in dragging the dust particles.

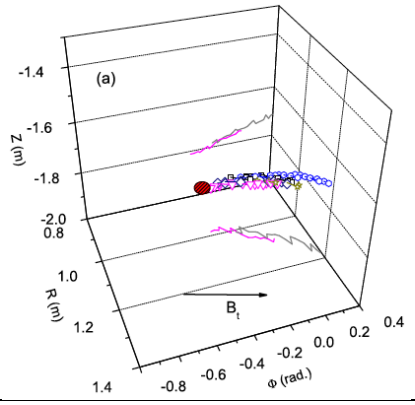

Fig. V.14. 3D trajectory of carbon dust particles recorded in the MAST tokamak. Reproduced with permission from [53], © IAEA 2010.

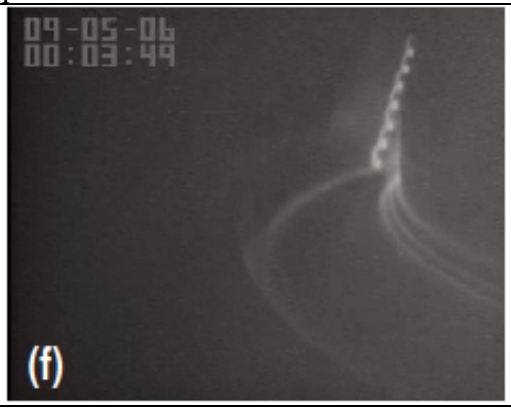

Fig. V.15. Spiral trajectory of a dust particle recorded in the DIII-D tokamak. Reproduced with permission from [12], © IAEA 2009.

Although fast cameras show that the majority of dust particles demonstrate rather smooth trajectories, some of the dust grains exhibit jitter-like deviation from the average direction of the trajectory [55], whereas some others have spiral-like trajectories (see Fig. V.15). We will see in the next section that such features can be explained by the non-spherical shape and agglomerate character of the grains. However, some movies recorded with fast cameras show that the dust grains can experience significant "kicks" by large blobs and ELM filaments.

A pattern recognition code developed and coupled to the fast camera imaging allows monitoring the dust mobilization rate (the number of new dust particles in tokamak volume per unit time), see [14] and the references therein. It was shown that for the carbon-based Tore Supra tokamak, the dust mobilization rate increases exponentially with the run-time (providing that no cleaning procedure is implemented), whereas in the ASDEX-U tokamak, with a tungsten first wall, the dust mobilization rate shows an initial strong reduction following the last ventilation event, and then it saturates [14]. In Tore Supra, most of the

mobilized dust was coming from carbon co-deposit layers. This finding looks beneficial for the ITER design, which has no carbon-based PFCs. However, much higher heat load in ITER can produce other sources of dust, which can be related to the melting of beryllium and tungsten armors.

Other experimental techniques (e.g. electrostatic dust detector, the capture of dust grains with aerogel, different gravimetric dust sensors, etc.) are also used for dust studies in magnetic fusion devices and the results found from the implementation of these techniques can be found in the review [15].

V.2. Theoretical aspects and numerical simulations of dust-related phenomena in magnetic fusion devices.

There is a large body of literature dedicated to the theoretical study of dust charging, forces, etc. in different environments ranging from laboratory experiments to astrophysics (see Refs. [56], [57], [58] and the references therein). However, in fusion plasma, the physics of dust has some important differences from what was studied in the laboratory experiments. First of all, unlike most of the laboratory experiments, the shape of the dust particles in fusion devices usually is far from spherical (recall Fig. V.3) and cannot be specified *a priori* (unless we are dealing with dedicated experiments, where well-characterized grains are injected into the fusion device). Next, the grain material of the dust particles in hot and dense fusion plasmas can be heated up to a very high temperature and dust ablation effects become important (recall the observations of dust particles with fast cameras discussed in Section V.1.3). As a result: i) the dust grains can change their shapes (e.g. metallic dust can melt), ii) the ablated material can form a "shield" altering the plasma-grain interactions, and iii) different plasma particle reflection coefficients and evaporation rates of different materials in the dust particles formed by agglomeration (recall Fig. V.10 (a)) can result in a "rocket force", which is virtually impossible to predict and characterize *a priori*. All of these issues make it difficult or even impossible to develop theoretical/computational tools that would describe the dust-related phenomena in the natural fusion plasma environment precisely. Nonetheless, benchmarking of the results of the dust dynamics simulations against the experimental data shows a reasonable agreement. It suggests that overall, the models used for the description of the dust-related phenomena in magnetic fusion devices capture at least the most important features of the dust-fusion plasma interactions.

V.2.1 Dust particle dynamics in fusion devices, theoretical approaches.

For stationary conditions, the flux of charged particles onto a dust grain immersed in the plasma should satisfy the ambipolarity conditions. Then for the case where there is no charge emission from the grain (e.g. thermionic of secondary electron emission), the dust grain usually becomes negatively charged to repel some electrons and equilibrate the fluxes of the "light" (and therefore "fast") electrons and the "heavy" (and therefore "slow") ions. For a spherical dust grain of a radius R_d, the grain charge number, Z_d, can be found from the following expression (e.g. see [56], [57], [58])

$$Z_d = \Lambda_d R_d T / e^2, \qquad (V.1)$$

where $\Lambda_d \sim 3$ is the numerical coefficient only weakly (logarithmically) depending on the plasma parameters and e is the elementary charge. We assume that the electron and ion temperatures are similar $T_e \sim T_i \sim T$. For $R_d \sim 1\,\mu m$ and $T \sim 10\,eV$ we find $Z_d \sim 10^4$. Due to the rather high plasma density, the charging time of the dust grains in fusion devices is very short, $\tau_{ch} \sim 10^{-8} s$ [36], so that dust charging can be considered in a quasi-stationary approximation.

The interaction of dust with the flow of homogeneous plasma having the velocity, $\vec{V}_p$, results in the drag force exerted on the grain

$$\vec{F}_{drag} = \varsigma_{drag} \pi R_d^2 M_i n_i V_{Ti} (\vec{V}_p - \vec{V}_d), \qquad (V.2)$$

where $\vec{V}_d$ is the dust grain velocity, M_i, n_i, and V_{Ti} are the ion mass, density, and thermal velocity respectively, and $\varsigma_{drag} \sim 10$ is a numerical factor that depends on the dust charge and plasma parameters, [57], [58].

Estimates from Ref. [36] show that the drag force is one of the dominant forces acting on the dust particles with $R_d \sim$ few μm at the edge of fusion plasmas (the divertor and SOL regions). This is because of the strong plasma flows existing in these regions due to plasma recycling and anomalous cross-field plasma transport. Under the drag force acceleration, the dust particles in fusion devices can be easily accelerated to ~100 m/s [15].

Apart from the drag force, other forces imposed on the dust particles in a fusion plasma are the electric, $eZ_d\vec{E}$, and Lorentz, $eZ_d(\vec{V}_d \times \vec{B})/c$, forces (here c is the light speed), the gravity force, the magnetic force acting on the grain having a magnetic moment, and some others. However, ferromagnetic materials are not used in the magnetic fusion devices so the magnetic force is unlikely to be important for the dynamics of dust naturally existing in the fusion plasmas. Moreover, estimates from [36] show that even though the dust charge number can be large, the ratio Z_d / M_d (determining the gyro-frequency of the dust particles) for micron-size grains is by orders of magnitude smaller than that for the plasma ions. Therefore, the Lorentz force can only alter the dynamics of very small (nano-scale) grains. Comparison of the electric and drag forces shows that for the edge plasmas in magnetic fusion devices they can only be comparable in the sheath region where the electric field is much stronger than that in the bulk of the edge plasma. Gravity usually becomes important for the grains with a characteristic size of over 100 μm [36]. Other forces acting on the grain, such as the thermal (or thermophoretic) forces related to the ion/neutral temperature inhomogeneity [59], [60] for the edge plasma conditions are usually smaller than the corresponding plasma and neutral gas drag forces.

However, the inhomogeneity of the material on the surface of a dust grain, which is rather typical for the agglomerated dust particles (recall Fig. V.10 (a)), can result in the so-called "rocket force" [36] related to the inhomogeneity of the coefficients of plasma particle reflection from the dust surface or the dust material ablation rate (for the case of strongly heated grains). In both cases, a strong unbalanced momentum flux can produce both a large force (comparable to or even exceeding the plasma drag force) and a torque acting on the agglomerated dust particles. It is plausible that the spiral trajectory of the dust particle shown

in Fig. V.15 is the result of such "rocket force" effects. Unfortunately, the existence of such effects is impossible to predict.

The expressions (which are rather cumbersome) for the dust grain charge, forces, heat flux and dust material temperature variation for spherical dust grains, relevant to the edge plasma conditions, can be found in [15].

However, all these expressions are only valid for spherical dust particles. The dynamics of non-spherical grains that are naturally present in the fusion devices (recall Fig. V.3) is more complex. For solid dust particles one should treat the grain dynamics as the motion of a rigid body:

$$M_d \frac{d\vec{V}_d}{dt} = \vec{F}_d, \tag{V.3}$$

$$\frac{d\vec{L}_d}{dt} = \vec{K}_d, \tag{V.4}$$

where M_d and $\vec{L}_d$ are the grain mass and angular momentum, whereas $\vec{F}_d$ and $\vec{K}_d$ are the force and torque acting on the grain.

In addition, one cannot describe any more grain charging with just the charge number Z_d but should consider the distribution of the charge over the grain surface, which, in particular, results in the departure of the force acting on the grain from Eq. (V.2). Therefore, strictly speaking, the exact analysis of the dynamics of non-spherical grains can be performed only numerically.

Even though rather comprehensive numerical simulations of the dust dynamics in fusion devices, which will be discussed in Section V.2.2, are based on the spherical dust particle approximation, it is important to have at least some estimate of the difference between the dynamics of the spherical and non-spherical grains.

Under the edge-plasma-relevant conditions, the dynamics of non-spherical grains can be analyzed by using symmetry principles. As an example, we follow [61] and consider the dynamics of a non-spherical grain in plasma without magnetic field. First, we assume that the angular velocity of the grain spinning, $\vec{\Omega}_d$, is relatively low, so that $|\vec{\Omega}_d|\tau_{ch} << 1$. Next, we will also assume that the speeds of the grain and the plasma flow are much lower than the thermal speed of the plasma ions (recall that we consider $T_e \sim T_i \sim T$), which means that $|\vec{V}_p|, |\vec{V}_d| << V_{Ti}$ and $|\vec{\Omega}_d|\ell_d << V_{Ti}$. Under such assumptions, both grain charging and the forces imposed on the grain can be considered in a quasi-stationary approximation. For the case where the properties of the grain surface responsible for the grain-plasma interactions are homogeneous, the directions of $\vec{F}_d$ and $\vec{K}_d$ will only depend on the directions of $\vec{W} \equiv \vec{V}_p - \vec{V}_d$, $\vec{\Omega}_d$ and the orientation of the grain. Moreover, for relatively small $|\vec{W}|$ and $|\vec{\Omega}_d|$ one can keep only a linear dependence of $\vec{F}_d$ and $\vec{K}_d$ on $\vec{W}$ and $\vec{\Omega}_d$. As a result, we have

$$(F_d)_\alpha = \Phi^{(W)}_{\alpha\beta} W_\beta + \Phi^{(\Omega)}_{\alpha\beta} (\Omega_d)_\beta, \tag{V.5}$$

$$(K_d)_\alpha = T^{(W)}_{\alpha\beta} W_\beta + T^{(\Omega)}_{\alpha\beta} (\Omega_d)_\beta, \tag{V.6}$$

where the tensors $\Phi_{\alpha\beta}^{(...)}$ and $T_{\alpha\beta}^{(...)}$ are determined only by the shape of the grain and the plasma parameters. For a general case, these tensors can only be calculated numerically. However, for the grain having rotational symmetry around some axis, the structure of the tensors $\Phi_{\alpha\beta}^{(...)}$ and $T_{\alpha\beta}^{(...)}$ can be found from geometrical arguments [61]. Indeed, for this case, the spatial orientation of the grain can be characterized by a dimensionless vector $\vec{D}$. Then, taking into account that $\vec{F}_d$, $\vec{D}$, and $\vec{W}$ are vectors, whereas $\vec{L}_d$, $\vec{K}_d$, and $\vec{\Omega}_d$ are pseudo-vectors, the most general form of the equations of motion of the grain can be written as follows

$$M_d \frac{d\vec{V}_d}{dt} = \Phi_1^{(W)}\vec{W} + \Phi_2^{(W)}\vec{D}(\vec{D}\cdot\vec{W}) + \Phi^{(\Omega)}(\vec{\Omega}_d \times \vec{D}) \quad , \tag{V.7}$$

$$\frac{d\vec{L}_d}{dt} = T^{(W)}(\vec{W}\times\vec{D}) + T_1^{(\Omega)}\vec{\Omega}_d + T_2^{(\Omega)}\vec{D}(\vec{D}\cdot\vec{\Omega}_d) \quad , \tag{V.8}$$

where $(L_d)_\alpha = I_{\alpha\beta}(\Omega_d)_\beta$ and $I_{\alpha\beta} = I_0\delta_{\alpha\beta} + I_1 D_\alpha D_\beta$ is the inertia tensor of the grain, where $\delta_{\alpha\beta}$ is the Kronecker delta and I_0 and I_1 describe the components of the inertia tensor. The scalars $\Phi_1^{(W)}$, $\Phi_2^{(W)}$, $\Phi^{(\Omega)}$, $T^{(W)}$, $T_1^{(\Omega)}$, and $T_2^{(\Omega)}$ are determined by particular properties of the grain material and shape and, for the grain shape not too far from spherical, can be estimated as $\Phi_1^{(W)} \sim \Phi_2^{(W)} \sim \hat{F}_d = \varsigma_{drag}\pi\ell_d^2 M_i n_i V_{Ti}$, $\Phi^{(\Omega)} \sim T^{(W)} \sim \hat{F}_d \ell_d$ and $T_1^{(\Omega)} \sim T_2^{(\Omega)} \sim \hat{F}_d \ell_d^2$.

As we see from Eq. (V.7), the force acting on a non-spherical grain is no longer aligned with the direction of the relative velocity $\vec{W}$, unlike the case of a spherical grain in Eq. (V.2). The departure is due to both the grain orientation and grain spinning (correspondingly the second and third terms on the right-hand side, RHS, of Eq. (V.7)). We notice that the second term was also derived in [62] from the direct calculation of the force acting on the grain for the combined Coulomb and dipole grain-plasma interaction potentials.

For the case $|\vec{V}_p| >> |\vec{V}_d|, |\vec{\Omega}_d|\ell_d$, Eq. (V.7, V.8) can be simplified and we have

$$M_d \frac{d\vec{V}_d}{dt} = \Phi_1^{(W)}\vec{V}_p + \Phi_2^{(W)}\vec{D}(\vec{D}\cdot\vec{V}_p) \quad , \tag{V.9}$$

$$\frac{d\vec{L}_d}{dt} = T^{(W)}(\vec{V}_p \times \vec{D}) \quad , \tag{V.10}$$

where Eq. (V.10) is identical to the equation describing the motion of symmetrical top in an effective gravity field $\propto \vec{V}_p$ [63]. The solution of Eq. (V.10) gives the oscillation of the vector $\vec{D}$ in time, which causes time oscillation of the force in Eq. (V.9) and, therefore, oscillations of the grain trajectory on a spatial scale Δ_d, which for the case of a "fast" top and relatively slow precession around the vector $\vec{V}_p$ can be large $\Delta_d \sim 1\,\text{cm} >> \ell_d$ (see [61]). It is plausible that the jittering of the grain trajectory observed in some cases by fast cameras is due to the non-sphericity of the grains.

Eqs. (V.6-V.10) describe the dynamics of non-spherical dust grains under the impact of the drag force associated with the plasma flow but with no effects of the magnetic field that is ubiquitous in the magnetic fusion devices. However, the impact of the magnetic field on the dust dynamics/spinning can be significant due to the dust grain interactions with the plasma. For example, in [64], [65] it was shown that gyration of the plasma particles and synergistic effects of the electric, $\vec{E}$, and magnetic, $\vec{B}$, fields can result in specific torques spinning up the dust particles. In [66] the approach developed in [61] was extended to the dynamics of non-spherical grains in the presence of a magnetic field and in [67] to the grains having some helical (propeller-like) features.

Overall, based on available results on the dynamics of non-spherical grains, we can conclude that in the absence of the "rocket force" effects, apart from some jittering (on the scale ~ 1 cm) of the dust particle trajectory, the dynamics of the spherical and non-spherical grains in fusion devices is rather similar. This justifies the applicability of the spherical grain approximation in numerical simulations. However, the dynamics of agglomerated dust particles can have a significant deviation from the predictions made with the spherical approximation.

As we have mentioned, the dust grains in fusion plasmas can be quickly heated up to high temperatures and start to ablate. We notice that the heat flux coming to the grain depends on grain charge, which can be affected by thermionic emission sensitive to the grain temperature. Such a nonlinear dependence of the heat flux to the grain on the grain temperature in some cases can cause a bifurcation phenomenon causing a sudden jump of the heat flux to the grain, the grain temperature and charge [68]. Dust ablation/evaporation is the mechanism of the reduction of the dust particle mass/size, which, in total, usually significantly exceeds the impact of dust material sputtering by the plasma ions impinging onto the grain. The plume of the ablated material can work as a shield reducing the heat flux coming to the grain from the ambient plasma in a way similar to the case of shielding of pellets injected into the core of the fusion plasma for fuelling purposes (e.g. see [69] and the references therein). However, it appears that significant shielding can only be formed for relatively large dust grains, $\ell_d \gtrsim \ell_{shield}$, where ℓ_{shield} depends on both the dust material and the plasma parameters [70], [71]. The reason for this is the fast initial expansion of the plume, which prevents the formation of the shield for small ℓ_d.

For $\ell_d > \ell_{shield}$ one should take into account the shielding effects. Numerical simulations show that an *ad hoc* reduction of the heat flux to the dust particles, imitating the shielding effect, has a very pronounced impact on plasma contamination with impurity because the shielded dust grains can penetrate deeper into the plasma which results in the increasing impurity concentration and radiation loss [72]. However, the models developed for the description of pellet shielding effects are focused on the interactions of the ablated material with hot ($T \gtrsim 1\,keV$) core plasma (see [73], [69], [74] and the references therein). The shielding effects in these models are described by the "stopping power" of the energetic electrons by the ablated material and no energy loss due to radiation of the ablated material is taken into account.

It is unlikely that this concept can be justified for shielding of high-Z dust particles in relatively cold ($T \lesssim 100\,eV$) edge plasma, where impurity radiation can effectively cool the ambient plasma. Therefore, in [75], [76], [77] a model was developed focused specifically on the shielding of high-Z (e.g. tungsten) dust grains in relatively cold edge plasmas, where

impurity radiation is one of the main ingredients resulting in the reduction of the heat flux coming to the grain. The dependence of the shielding factor, γ_{shield}, which is the ratio of the heat flux to the grain with and without shielding effects, on the plasma parameters can be found in the corresponding references.

Another important issue related to the dust dynamics in fusion devices is the dust collisions with the plasma-facing components, which is quite often observed with fast cameras (recall Fig. V.13). Such collisions of negatively charged grains are only possible when the grain kinetic energy normal to the surface exceeds the repulsive electrostatic sheath potential barrier (which is usually not the case in the laboratory dusty plasma experiments [58]). Estimations show that to overcome such a potential barrier for a micron-size particle, the normal component of its velocity should exceed (depending on the dust material) ~1-5 m/s [36], [15], which is much lower than the typical speed of the dust in fusion devices ~ 100 m/s. Different models of dust-wall collisions are used in numerical simulations of the dust dynamics. These models range from simple reflection coefficients [37], [78] to the rather sophisticated Thornton-Ning model [79] for the sticking and bouncing of adhesive, elastic-plastic spheres (e.g. see [80]).

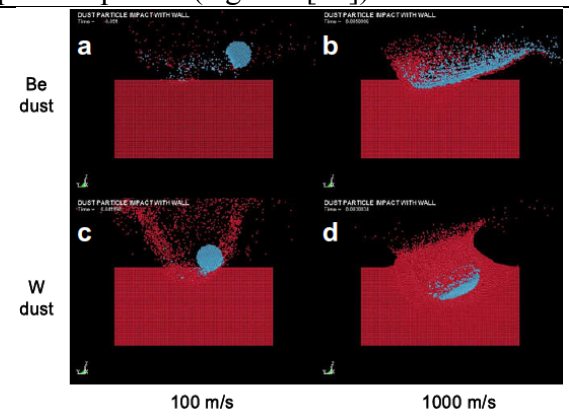

Fig. V.16. Simulated impact of beryllium and tungsten dust particles of 0.5 μm radius (blue) on beryllium target (red) at speeds 10^2 (a, c) and 10^3 m/s (b, d), and impact angle of 45°. Reproduced with permission from [82], © Elseiver 2009.

Potentially, the dust collisions with the PFCs can have a large impact on both the dust dynamics and wall erosion. In particular, the dust grain can be disintegrated in the course of the collision, as observed in experiments (recall Fig.V.11), and also can contribute significantly to erosion and surface morphology modification of the PFC's materials. Numerical simulations of the collisions of dust grains with PFCs can be performed by using the commercial finite element code for structural analysis, LS-DYNA [81]. The LS-DYNA code solves three-dimensional transient multi-physics problems including solid mechanics, deformation, contacts, fragmentation, heat transfer, etc., and implements a large variety of material models and simulation techniques. Therefore, this code can provide, presumably, the most accurate assessment of the results of the dust collision with the PFCs. The results of such simulations of the collisions of beryllium and tungsten dust particles of 0.5 μm radius, impinging onto a beryllium target at 45°, is presented in Fig. V.16. As one can see, at a relatively low speed both beryllium and tungsten grains are bouncing off the target with very little impact on both the grains and the target. However, at high speed, the beryllium grain disintegrates completely during the collision but still produces very modest target erosion, whereas the fast tungsten particle creates quite a deep crater in the target and produces a large amount of debris.

V.2.2 Numerical simulations of dust particle dynamics and dust impact on edge plasma parameters.

The dynamics of dust particles in fusion edge plasma having strongly inhomogeneous parameters is very complex. Therefore, the study of the dust dynamics in real fusion devices and assessment of a self-consistent impact of the dust on the edge plasma can only be done numerically. Up to now, few codes DUSTT [78], [68], DTOKS [83], [84], MIGRAINE [85], [80], and DUMBO [52] have been developed for these purposes. All these codes implement more or less similar models of dust grain charging and forces imposed by the dust-plasma interactions, which are considered by using the spherical grain approximation. However, some details of these codes have significant differences, which can alter some features of the dust dynamics. For example, currently, only the DUSTT code accounts for the shielding effects, which slow down the dust grain ablation/evaporation and affect the dust penetration depth into the edge plasma and, therefore, the impurity concentration and radiation loss. On the other hand, MIGRAINE employs a rather sophisticated model describing the dust collisions with the plasma-facing components, which goes far beyond the simple reflection coefficients used in other codes (e.g. in DUSTT) and, therefore, is better suitable for the study of dust mobilization from the material surfaces. All of these codes were developed for dust studies in tokamaks and, therefore, assume the toroidal symmetry of the plasma parameters. But, the DUSTT code has been modified recently and is now used for the study of dust dynamics in the helical device LHD [51]. The plasma parameters used in all of these codes focused on dust dynamics studies come either from experimental measurements or, in most cases, from 2D edge plasma transport codes (e.g. see [86]) such as UEDGE [87], different versions of the SOLPS code (e.g. see [88] and the references therein), and some others.

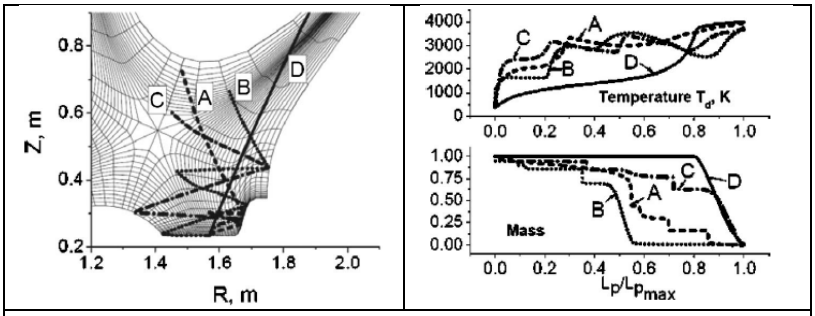

Fig. V.17. Poloidal projection (left) of 1 μm carbon dust particle trajectories. Dust grains were launched into DIII-D from outer strike point with velocities 10 (A), 10^2 (B), 10^3 (C), and 10^4 cm/s. and dust grain temperatures and relative mass (right) as a function of poloidal distance traveled. Reproduced with permission from [78], © AIP Publishing 2005.

A few examples of dust trajectories found from the numerical simulations of the dust dynamics for prescribed edge plasma parameters are shown in Figs. V.17-V.18. We notice that a sharp zigzag in the middle of the divertor volume of particle B in Fig. V.17 is just a visual effect of the 3D trajectory projected on 2D poloidal coordinates. Similar effects are also seen in the poloidal projection of dust trajectories in Fig. V.18. However, the reversal of the toroidal direction of dust propagation seen in Fig. V.18 is due to the different directions of the toroidal components of the plasma flow in the divertor regions of the outer and inner SOL [37]. A similar change of the toroidal direction of the dust motion was also observed in numerical simulations (e.g. see [68]) and by fast cameras for the case where the dust grain moves from one divertor to the other (e.g. see Refs. [49], [12]]).

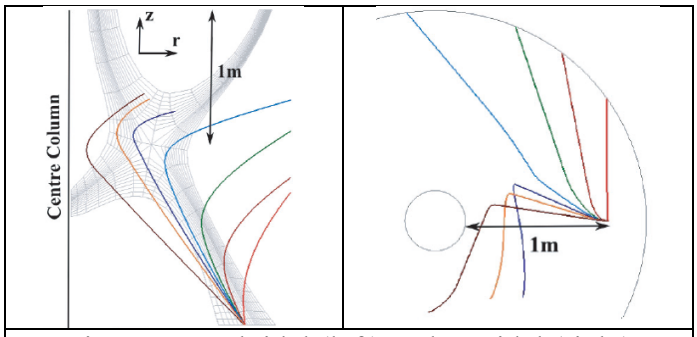

Fig. V.18. Poloidal (left) and toroidal (right) projections of 1 μm carbon dust particle trajectories. Grains were launched into MAST from outer strike point with velocity 30 m/s and different angles. Reproduced with permission from [83], © IOP Publishing 2008.

However, a considerable amount of dust injected into a fusion device can significantly alter the plasma parameters and even cause termination of the discharge (recall Fig. V.1 and see Refs [4], [5]). The numerical simulations performed in Ref. [78] for two cases of impurity injection into the plasma of (a) neutral atoms and (b) dust particles have shown a large difference in the edge plasma parameters even though the rate of impurity mass injection was the same in both cases. However, for accurate assessment of the dust impact on the edge plasma for the case of a relatively high dust injection rate, one should take into account the self-consistent variation of both the plasma parameters, caused by the impurity provided by the dust, and the dust dynamics and transport in dust impurity-modified plasma environment.

Such self-consistent consideration became possible after the coupling of the dust and edge plasma transport codes DUSTT and UEDGE into DUSTT-UEDGE package [55]. This package allows considering different scenarios of dust injection into plasma. For example, all designated dust grains can be injected within a short time, simulating a "spark" event shown in Fig.V.1, or the grains can be injected into the plasma continuously. We notice that the DUSTT-UEDGE package allows choosing the distribution of dust injection location over the PFCs surfaces and distribution of the dust grains in the injection velocity and size.

In Fig.V.19-V.20 one can see the results of simulations with the DUSTT-UEDGE package of continuous injection of tungsten dust into the ITER plasma [72].

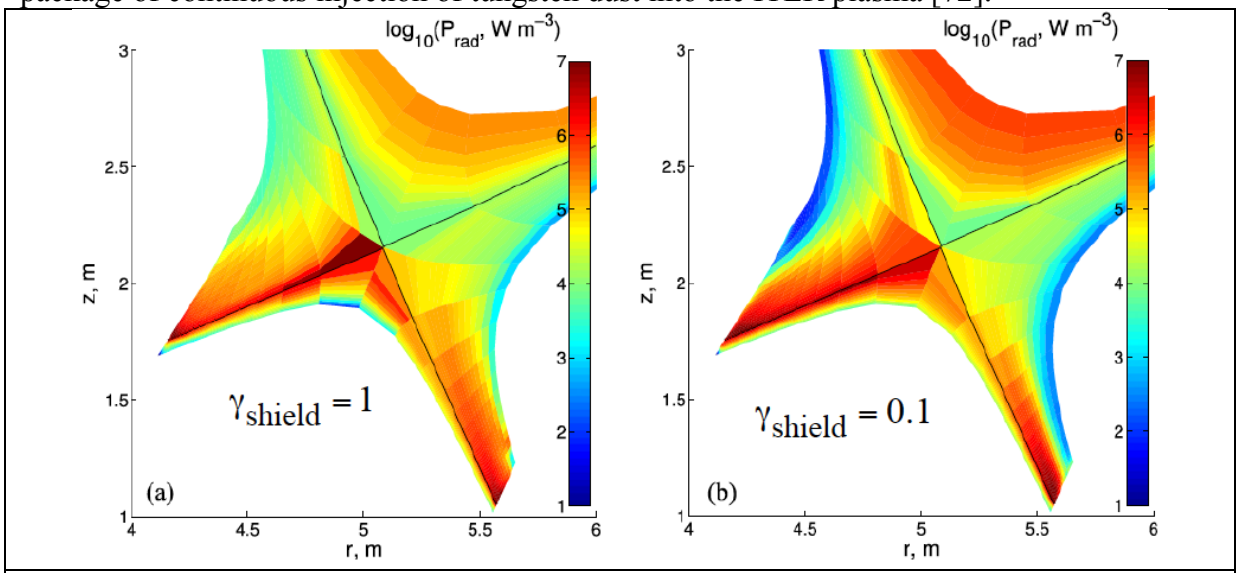

Fig.V.19. Tungsten impurity radiation distribution in the ITER divertor for 10 μm dust grain injection with the mass rate of 60 mg/s for different shielding factors. Reproduced with permission from [72], © AIP Publishing 2015.

As one can see from Fig.V.19(b), the tungsten radiation loss strongly increases at the core-edge interface as a result of deeper penetration of dust into the core plasma when the shielding effects are taken into account. Another illustration of shielding effects can be found in Fig.V.20. Taking into account that ITER assumes to use impurity seeding to reach the semi-detached state in the outer divertor, the data from Fig.V.20 suggest that to avoid possible termination of the discharge due to thermal collapse, the mass rate by continuous injection of tungsten dust into ITER plasma should not exceed ~30 mg/s.

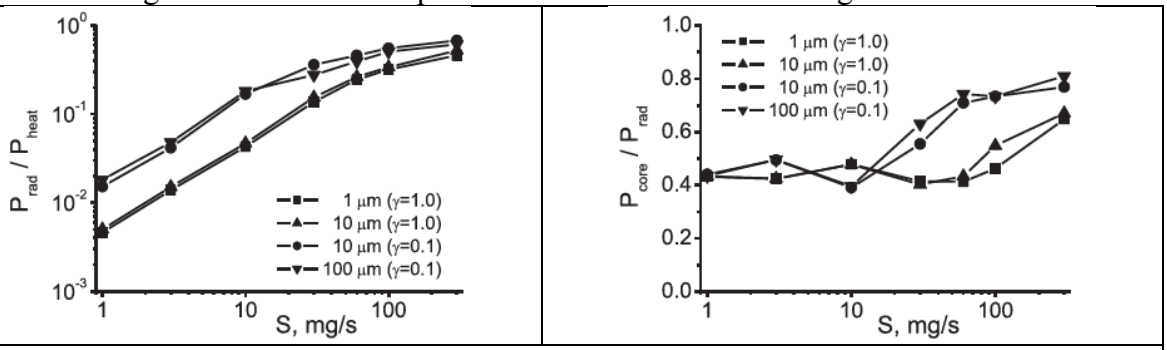

Fig.V.20. Normalized tungsten radiation power (left) and fraction of the tungsten-radiated power from the core-edge region (right) as functions of the dust mass injection rate for different grain radii and shielding factor. Reproduced with permission from [72], © AIP Publishing 2015.

However, to this moment we have no simulation results on the tolerable amount of the tungsten dust injected into the ITER plasma on a short (e.g. ~1 ms) time scale. The reason for this is the computational challenge related to the fast and spatially localized change of the plasma parameters, which accompanies such a dust injection scenario.

Conclusions for Chapter V

As we have seen, the study of the dust in fusion devices brings together the edge plasma physics and the material and surface physics of the PFC materials. In the last 10-15 years, the study of the dust physics in fusion devices has developed into a separate research area, which is recognized by the plasma fusion community as important for future magnetic fusion reactors. Over that time, many new diagnostic tools for *in situ* dust studies have been developed and implemented on the magnetic fusion devices (e.g. laser scattering, pattern recognition with fast cameras, etc.). Theoretical study of the dust dynamics in fusion devices greatly benefits from the models of the dust-plasma interactions developed previously for different applications (e.g. see Refs. [56], [57], [58] and the references therein). These models have been partly extended to non-spherical grains, which allowed assessing the impact of complex shapes of the dust particles in fusion devices on the dust dynamics. The results of numerical simulations (performed with sophisticated codes developed from scratch) of the dust particle dynamics and transport in fusion devices show decent agreement with the experimental observations.

However, there are still some gaps in our understanding/description of the dust physics in fusion devices. Some of them are related to the plasma physics (e.g. the description of an impact of large turbulent plasma fluctuations, often observed in the edge plasma, on dust transport), but probably the most important and the most complex one, the

dust generation and injection rate into the plasma, is related to both the material science and the plasma-material interactions. Still, a lot should be done in this direction.

References for Chapter V

[1] T. Ohkawa "Dust Particles as a Possible Source of Impurities in Tokamaks", Kakuyugo Kenkyu **37** (1977) 117-131

[2] R. Behrisch, R. S. Blewer, H. Kukral, B. M. U. Scherzer, H. Schnidl, P. Staib, G. Staudenmaier, and Group de TFR, "Spatial distribution of limiter material and impurities on the first wall of TFR 400", J. Nucl. Mater. **76-78** (1978) 437-444

[3] D. H. J. Goodall "High speed cine film studies of plasma behaviour and plasma-surface interactions in tokamaks", J. Nucl. Mater. **111-112** (1982) 11-22

[4] J. C. Flanagan, M. Sertoli, M. Bacharis, G. F. Matthews, P. C. de Vries, A. Widdowson, I. H. Coffey, G. Arnoux, B. Sieglin, S. Brezinsek, J. W. Coenen, S. Marsen, T. Craciunescu, A. Murari, D. Harting, A. Cackett, E. Hodille and JET-EFDA Contributors, "Characterising dust in JET with the new ITER-like wall", Plasma Phys. Contr. Fusion **57** (2015) 014037.

[5] M. Sertoli, J. C. Flanagan, M. Bacharis, O. Kardaun, A. Jarvinen, G. F. Matthews, S. Brezinsek, D. Harting, A. Cackett, E. Hodille, I. H. Coffey, E. Lazzaro, T. Pütterich, JET-EFDA Contributors, "Impact of W events and dust on JET-ILW operation", J. Nucl. Mater. **463** (2015) 837-841.

[6] K. Saito, T. Mutoh, R. Kumazawa, T. Seki, Y. Nakamura, N. Ashikawa, K. Sato, M. Shoji, S. Masuzaki, T. Watari, H. Ogawa, H. Takeuchi, H. Kasahara, F. Shimpo, G. Nomura, M. Yokota, C. Takahashi, A. Komori, Y. Zhao, J.S. Yoon, J.G. Kwak, The LHD Experimental Group "ICRF long-pulse discharge and interaction with a chamber wall and antennas in LHD" J. Nucl. Mater. **363-365** (2007) 1323-1328.

[7] J. Winter "Dust in fusion devices - experimental evidence, possible sources and consequences", Plasma Phys. Control. Fusion **40** (1998) 1201-1210

[8] G. Federici, C.H. Skinner, J.N. Brooks, J.P. Coad, C. Grisolia, A.A. Haasz, A. Hassanein, V. Philipps, C.S. Pitcher, J. Roth, W.R. Wampler and D.G. Whyte "Plasma-material interactions in current tokamaks and their implications for next step fusion reactors", Nucl. Fusion **41** (2001) 1967-2137

[9] J. Winter "Dust in fusion devices - a multi-faceted problem connecting high- and low-temperature plasma physics", Plasma Phys. Contr. Fusion **46** (2004) B583-B592

[10] J.Ph. Girard, W. Gulden, B. Kolbasov, A.-J. Louzeiro-Malaquias, D. Pettis and L. Rodriguez-Rodrigo, "Summary of the 8th IAEA Technical Meeting on Fusion Power Plant Safety", Nucl. Fusion **48** (2008) 015008

[11] A. E. Costley, T. Sugie, G. Vayakis, C. I. Walker "Technological challenges of ITER diagnostics", Fus. Eng. Des. **74** (2005) 109-119

[12] D. L. Rudakov, A. Litnovsky, W. P.West, J. H. Yu, J. A. Boedo, B. D. Bray, S. Brezinsek, N. H. Brooks, M. E. Fenstermacher, M. Groth, E. M. Hollmann, A. Huber, A. W. Hyatt, S. I. Krasheninnikov, C. J. Lasnier, A. G. McLean, R. A. Moyer, A. Yu. Pigarov, V. Philipps, A. Pospieszczyk, R. D. Smirnov, J. P. Sharpe, W. M. Solomon, J. G.Watkins and C. P. C. Wong "Dust studies in DIII-D and TEXTOR", Nucl. Fusion **49** (2009) 085022

[13] W. P. West, B. D. Bray, "Correlation of submicron dust observed in DIII-D during plasma operation with plasma operating parameters", J. Nucl. Mater. **363-365** (2007) 107-111.

[14] Suk-Ho Hong, Ch. Grisolia, V. Rohde, P. Monier-Garbet, Tore Supra Team and ASDEX Upgrade Team "Temporal evolution and spatial distribution of dust creation events in

Tore Supra and in ASDEX Upgrade studied by CCD image analysis", Nucl. Fusion **50** (2010) 035002.
[15] S. I. Krasheninnikov, R. D. Smirnov and D. L. Rudakov "Dust in magnetic fusion devices", Plasma Phys. Control. Fusion **53** (2011) 083001.
[16] C. Arnas , J. Irby, S. Celli, G. De Temmerman, Y. Addab, L. Couëdel, C. Grisolia, Y. Lin, C. Martin, C. Pardanaud, S. Pierson, "Characterization and origin of large size dust particles produced in the Alcator C-Mod tokamak" Nucl. Mater. Energy **11** (2017) 12-19
[17] F. Brochard, A. Shalpegin, S. Bardin, T. Lunt, V. Rohde, J.L. Briançon, G. Pautasso, C. Vorpahl, R. Neu and The ASDEX Upgrade Team "Video analysis of dust events in full-tungsten ASDEX Upgrade", Nucl. Fusion **57** (2017) 036002
[18] E. Fortuna-Zaleśna, J. Grzonka, M. Rubel, A. Garcia-Carrasco, A. Widdowson, A. Baron-Wieche, L. Ciupiński, JET Contributors, "Studies of dust from JET with the ITER-Like Wall: Composition and internal structure" Nucl. Mater. Energy **12** (2017) 582-587
[19] J. P. Sharpe, D. A. Petti, H.-W. Bartels, "A review of dust in fusion devices: Implications for safety and operational performance", Fusion Eng. Des. **63-64** (2002) 153-163
[20] K. Koga, S. Iwashita, S. Kiridoshi, M. Shiratani, N. Ashikawa, K. Nishimura, A. Sagara, A. Komori and LND Experimental Group, "Characterization of Dust Particles Ranging in Size from1nm to 10μm Collected in the LHD", Plasma and Fusion Res. **4** (2009) 034.
[21] Ph. Chappuis, E. Tsitrone, M. Mayne, X. Armand, H. Linke, H. Bolt, D. Petti, J. P. Sharpe, "Dust characterization and analysis in Tore-Supra", J. Nucl. Mater. **290-293** (2001) 245-249.
[22] W. P. West, B. D. Bray and J. Burkart, "Measurement of number density and size distribution of dust in DIII-D during normal plasma operation", Plasma Phys. Contr. Fusion **48** (2006) 1661-1672.
[23] A. A. Tuccillo, A. Alekseyev, B. Angelini, S. V. Annibaldi, M. L. Apicella, G. Apruzzese, J. Berrino, E. Barbato, A. Bertocchi, A. Biancalani, W. Bin, A. Botrugno, G. Bracco, S. Briguglio, A. Bruschi, P. Buratti, G. Calabrò, A. Cardinali, C. Castaldo, C. Centioli, R. Cesario, L. Chen, S. Cirant, V. Cocilovo, F. Crisanti, R. De Angelis, U. de Angelis, L. Di Matteo, C. Di Troia, B. Esposito, G. Fogaccia, D. Frigione, L. Gabellieri, F. Gandini, E. Giovannozzi, G. Granucci, F. Gravanti, G. Grossetti, G. Grosso, F. Iannone, H. Kroegler, V. Lazarev, E. Lazzaro, I. E. Lyublinski, G. Maddaluno, M. Marinucci, D. Marocco, J. R. Martin-Solis, G. Mazzitelli, C. Mazzotta, V. Mellera, F. Mirizzi, S. Mirnov, G. Monari, A. Moro, V. Muzzini, S. Nowak, F. P. Orsitto, L. Panaccione, D. Pacella, M. Panella, F. Pegoraro, V. Pericoli-Ridolfini, S. Podda, S. Ratynskaia, G. Ravera, A. Romano, A. Rufoloni, A. Simonetto, P. Smeulders, C. Sozzi, E. Sternini, B. Tilia, O. Tudisco, A. Vertkov, V. Vitale, G. Vlad, R. Zagórski, M. Zerbini and F. Zonca, "Overview of the FTU results", Nucl. Fusion **49** (2009) 104013.
[24] E. Giovannozzi , M. Beurskens , M. Kempenaars , R. Pasqualotto , A. Rydzy , and JET EFDA Contributors, "Detection of dust on JET with the high resolution Thomson scattering system", Rev. Sci. Instr. **81** (2010) 10E131.
[25] R. D. Smirnov, W. P. West, S. I. Krasheninnikov, A. Yu. Pigarov, and M. Rosenberg, B. D. Bray "Laser-dust interaction and dust size distribution measurements on DIII-D", Phys. Plasmas **14** (2007) 112507.

[26] R. D. Smirnov, S. I. Krasheninnikov, J. H. Yu, A. Yu. Pigarov, M. Rosenberg and J L Terry, "On visibility of carbon dust particles in fusion plasmas with fast framing cameras", Plasma Phys. Contr. Fusion **51** (2009) 055017.
[27] J. H. Yu, D. L. Rudakov, A. Yu. Pigarov, R. D. Smirnov, N. H. Brooks, S. H. Muller, W. P. West, "Fast camera imaging of dust in the DIII-D tokamak" J. Nucl. Mater. **390-391** (2009) 216-219.
[28] B. D. Bray, W. P. West, D. Rudakov, "Correlation of submicron dust production in DIII-D to impulsive wall heating from ELMs", J. Nucl. Mater. **390-391** (2009) 96-99.
[29] E. Fortuna-Zalesna, J. Grzonka, M. Rasinski, M. Balden, V. Rohde, K. J. Kurzydlowski and the ASDEX Upgrade Team "Characterization of dust collected after plasma operation of all-tungsten ASDEX Upgrade", Phys. Scr. **T159** (2014) 014066.
[30] M. De Angeli, G. Maddulano, L. Laguardia, D. Ripamonti, E. Perelli Cippo, M. L. Apicella, C. Conti, G. Giacomi, F. Grosso, "Dust characterization in FTU tokamak", J. Nucl. Mater. **463** (2015) 847-850.
[31] E. Fortuna-Zaleśna, J. Grzonka, M. Rubel, A. Garcia-Carrasco, A. Widdowson, A. Baron-Wiechec, L. Ciupiński, JET Contributors, "Studies of dust from JET with the ITER-Like Wall: Composition and internal structure", Nucl. Mater. Energy **12** (2017) 582-587.
[32] V. Rohde, N. Endstrasser, U.v. Toussaint, M. Balden, T. Lunt, R. Neu, A. Hakola, J. Bucalossi, ASDEX Upgrade Team, "Thungsten erosion by arcs in ASDEX Upgrade", J. Nucl. Mater. **415** (2011) S46-S50.
[33] S. Kajita, M. Fukumoto, M. Tokitani, T. Nakano, Y. Noiri, N. Ohno, S. Masuzaki, S. Takamura, N. Yoshida and Y. Ueda, "Impact of arcing on carbon and tungsten: from the observations in JT-60U, LHD and NAGDIS-II", Nucl. Fusion **53** (2013) 053013.
[34] D. L. Rudakov, C. P. Chrobak, R. P. Doerner, S. I. Krasheninnikov, R. A. Moyer, K. R. Umstadter, W. R. Wampler, C. P. C. Wong "Arcing and its role in PFC erosion and dust production in DIII-D", J. Nucl. Mater. **438** (2013) S805-S808.
[35] A. Baron-Wiechec, E. Fortuna-Zaleśna, J. Grzonka, M. Rubel, A. Widdowson, C. Ayres, J. P. Coad, C. Hardie, K. Heinola, G. F. Matthews and JET Contributors, "First dust study in JET with the ITER-like wall: sampling, analysis and classification", Nucl. Fusion **55** (2015) 113033
[36] S. I. Krasheninnikov, Y. Tomita, R. D. Smirnov, and R. K. Janev, "On dust dynamics in tokamak edge plasmas", Phys. Plasmas **11** (2004) 3141-3150.
[37] S. I. Krasheninnikov and T. K. Soboleva, "Dynamics and transport of dust particles in tokamak edge plasmas", Plasma Phys. Control. Fusion **47** (2005) A339-A352.
[38] D. L. Rudakov, W. P. West, C. P. C. Wong, N. H. Brooks, T. E. Evans, M. E. Fenstermacher, M. Groth, S. I. Krasheninnikov, C. J. Lasnier, A. G. McLean, A. Yu. Pigarov, W. M. Solomon, G. Y. Antar, J. A. Boedo, R. P. Doerner, E. M. Hollmann, A. W. Hyatt, R. A. Moyer, J. G. Watkins, "Migration of artificially introduced micron-size carbon dust in the DIII-D divertor", J. Nucl. Mater. **363-365** (2007) 227-232.
[39] P. Tolias, S. Ratynskaia, M. De Angeli, G. De Temmerman, D. Ripamonti, G. Riva, I. Bykov, A. Shalpegin, L. Vignitchouk, F. Brochard, K. Bystrov, S Bardin and A Litnovsky, "Dust remobilization in fusion plasmas under steady state conditions", Plasma Phys. Control. Fusion **58** (2016) 025009.

[40] D. G. Whyte, T. E. Evans, C. P. C. Wong, W. P. West, R. Bastasz, J. P. Allain, J.N. Brooks, "Experimental observations of lithium as a plasma-facing surface in the DIII-D tokamak divertor", Fusion Eng. Des. **72** (2004) 133–147

[41] N. Klimov, V. Podkovyrov, A. Zhitlukhin, D. Kovalenko, B. Bazylev, G. Janeschitz, I. Landman, S. Pestchanyi, G. Federici, A. Loarte, M. Merola, J. Linke, T. Hirai, J. Compan, "Experimental study of PFCs erosion under ITER-like transient loads at plasma gun facility QSPA", J. Nucl. Mater. **390-391** (2009) 721-726.

[42] J. W. Coenen, B. Bazylev, S. Brezinsek, V. Philipps, T. Hirai, A. Kreter, J. Linke, G. Sergienko, A. Pospieszczyk, T. Tanabe, Y. Ueda, U. Samm, The TEXTOR-Team "Tungsten melt layer motion and splashing on castellated tungsten surfaces at the tokamak TEXTOR" J. Nucl. Mater. **415** (2011) S78-S82.

[43] G. De Temmerman, J. Daniels, K. Bystrov, M. A. van den Berg and J. J. Zielinski, "Melt-layer motion and droplet ejection under divertor-relevant plasma conditions", Nucl. Fusion **53** (2013) 023008.

[44] V. A. Makhlaj, I. E. Garkusha, N. N. Aksenov, A. A. Chuvilo, V. V. Chebotarev, I. Landman, S. V. Malykhin, S. Pestchanyi, A. T. Pugachov, "Dust generation mechanisms under powerful plasma impacts to the tungsten surfaces in ITER ELM simulation experiments", J. Nucl. Mater. **438** (2013) S233-S236.

[45] A. A. Vasilyev, A. S. Arakcheev, I. A. Bataev, V. A. Bataev, A. V. Burdakov, I. V. Kandaurov, A. A. Kasatov, V. V. Kurkuchekov, K. I. Mekler, V. A. Popov, A. A. Shoshin, D. I. Skovorodin, Yu. A. Trunev, L .N. Vyacheslavov, "In-situ imaging of tungsten surface modification under ITER-like transient heat loads", Nucl. Mater. Energy **12** (2017) 553-558.

[46] A. Shalpegin, F. Brochard, S. Ratynskaia, P. Tolias, M. De Angeli, L. Vignitchouk, I. Bykov, S. Bardin, K. Bystrov, T. Morgan and G. De Temmerman, "Highly resolved measurements of dust motion in the sheath boundary of magnetized plasmas", Nucl. Fusion **55** (2015) 112001.

[47] S. Ratynskaia, C. Castaldo, E. Giovannozzi, D. Rudakov, G. Morfill, M. Horanyi, J. H. Yu and G. Maddaluno, "*In situ* dust detection in fusion devices", Plasma Phys. Contr. Fusion **50** (2008) 124046

[48] R. J. Maqueda, G. A. Wurden, "Fast imaging of visible phenomena in TFTR", Nucl. Fusion **39** (1999) 629-636

[49] A. L. Roquemore, N. Nishino, C. H. Skinner, C. Bush, R. Kaita, R. Maqueda, W. Davis, A. Yu Pigarov, S. I. Krasheninnikov, "3D measurements of mobile dust particle trajectories in NSTX", J. Nucl. Mater. **363-365** (2007) 222-226.

[50] M. Tang, J. S. Hu, J. G. Li, Y.-F. Li, G. Morfill, N. Ashikawa, "Recent researches on dust in EAST and HT-7 tokamaks", J. Nucl. Mater. **415** (2011) S1094-1097

[51] M. Shoji, S. Masuzaki, Y. Tanaka, A.Yu. Pigarov, R.D. Smirnov, G. Kawamura, Y. Uesugi, H. Yamada, The LHD Experiment Group, "Analysis of the three-dimensional trajectories of dusts observed with a stereoscopic fast framing camera in the Large Helical Device", J. Nucl. Mater. **463** (2015) 861-864.

[52] A. Autricque, S. H. Hong, N. Fedorczak, S.H. Son, H.Y. Lee, I. Song, W. Choe, C. Grisolia, "Simulation of W dust transport in the KSTAR tokamak, comparison with fast camera data", Nucl. Mater. Energy **12** (2017) 599-604.

[53] G. De Temmerman, M. Bacharis, J. Dowling and S. Lisgo, "Dust creation and transport in MAST", Nucl. Fusion **50** (2010) 105012.

[54] Suk-Ho Hong, K.-R. Kim, W.-H. Ko, Yong-Un Nam, "Quantitative measurement of in-vessel dust velocity and its correlation with toroidal rotation of plasmas", J. Nucl. Mater **463** (2015) 851-855.
[55] R. D. Smirnov, S. I. Krasheninnikov, A. Yu. Pigarov, A. L. Roquemore, D. K. Mansfield, J. Nichols, "Modeling of dust impact on tokamak edge plasmas", J. Nucl. Mater. **415** (2011) S1067-S1072.
[56] V. N. Tsytovich "Dust plasma crystal, drops, and clouds", Physiscs-Uspekhi **40** (1997) 53-94
[57] P. K. Shukla and A. A. Mamun, "Introduction to Dusty Plasma Physics", Bristol: Institute of Physics Publishing, 2002.
[58] V. E. Fortov and G. E. Morfill (ed) "Complex and Dusty Plasmas", Boca Raton, FL: CRC Press, 2010.
[59] L. Talbot, R. K. Cheng, R. W. Schefer and D. R. Willis, "Thermophoresis of particles in a heated boundary layer", J. Fluid Mech. **101** (1980) 737-758.
[60] A. A. Stepanenko, R. D. Smirnov, V. M. Zhdanov, and S. I. Krasheninnikov, "On the thermal force acting on dust grain in fully ionize", Phys. Plasmas **18** (2011) 033702.
[61] S. I. Krasheninnikov, "On the dynamics of nonspherical dust grain in plasma" Phys. Plasmas **17** (2010) 033703.
[62] S. I. Krasheninnikov and D. A. Mendis, "On the drag force on non-spherical dust grain" J. Plasma Phys. **77** (2011) 271-276.
[63] L. D. Landau and E. M. Lifshits, Course of Theoretical Physics (Elsevier, Amsterdam, 2003), Vol. 1, p. 112.
[64] S. I. Krasheninnikov, "On dust spin up in uniform magnetized plasma", Phys. Plasmas **13** (2006) 114502.
[65] S. I. Krasheninnikov, V. I. Shevchenko, P. K. Shukla "Spinning of a charged dust particle in a magnetized plasma", Phys. Lett. A **361** (2007) 133-135.
[66] A. A. Stepanenko and S. I. Krasheninnikov, "On the theory of dynamics of dust grain in plasma", Phys. Plasmas **20** (2013) 033702.
[67] S. I. Krasheninnikov, "On the dynamics of propeller-like dust grain in plasma", Phys. Plasmas **20** (2013) 114502.

[68] R. D. Smirnov, A. Yu. Pigarov, M. Rosenberg, S. I. Krasheninnikov and D. A. Mendis, "Modelling of dynamics and transport of carbon dust particles in tokamaks", Plasma Phys. Contr. Fusion **49** (2007) 347-371.
[69] S. L. Milora, W. A. Houlberg, L. L. Lengyel and V. Mertens, "Pellet Fuelling", Nucl. Fusion **35** (1995) 657-754.
[70] S. I. Krasheninnikov and R. D. Smirnov, "On interaction of large dust grains with fusion plasma", Phys. Plasmas **16** (2009) 114501.
[71] B. T. Brown, R. D. Smirnov, and S. I. Krasheninnikov, "On vapor shielding of dust grains of iron, molybdenum, and tungsten in fusion plasmas", Phys. Plasmas **21** (2014) 024501.
[72] R. D. Smirnov, S. I. Krasheninnikov, A. Yu. Pigarov, T. D. Rognlien, "Tungsten dust impact on ITER-like plasma edge", Phys. Plasmas **22** (2015) 012506.
[73] P. B. Parks, R. J. Turnbull, and C. A. Foster, "A model for the ablation rate of a solid hydrogen pellet in a plasma", Nucl. Fusion **17** (1977) 539-556.

[74] V. A. Rozhansky and I. Yu. Senichenkov, "On the ablation models of fuel pellets" Plasma Phys. Rep. **31** (2005) 993-1002.
[75] E. D. Marenkov and S. I. Krasheninnikov, "Ablation of high-Z material dust grains in edge plasmas of magnetic fusion devices", Phys. Plasmas **21** (2014) 123701.
[76] S. I. Krasheninnikov and E. D. Marenkov, "On ablation of large Tungsten dust grains in edge plasma of fusion devices", J. Nucl. Mater. **463** (2015) 869-872.
[77] R. D. Smirnov and S. I. Krasheninnikov, "Impact of cross-field motion on ablation of high-Z dust in fusion edge plasmas", Phys. Plasmas **24** (2017) 072505.
[78] A. Yu. Pigarov, S. I. Krasheninnikov, T. K. Soboleva, and T. D. Rognlien, "Dust-particle transport in tokamak edge plasmas", Phys. Plasmas **12** (2005) 122508.
[79] C. Thornton, Z. Ning, "A theoretical model for the stick/bounce behavior of advesive, elastic-plastic spheres", Powder Techn. **99** (1998) 154-162.
[80] L. Vignitchouk, P. Tolias and S. Ratynskaia, "Dust–wall and dust–plasma interaction in the MIGRAINe code", Plasma Phys. Control. Fusion **56** (2014) 095005.
[81] <http://www.lstc.com/lsdyna.htm>.
[82] R. D. Smirnov, S. I. Krasheninnikov, A. Yu. Pigarov, D. J. Benson, M. Rosenberg, D. A. Mendis, J. Nucl. Mater. **390-391** (2009) 84-87.
[83] J. D. Martin, M. Bacharis, M. Coppins, G. F. Counsell and J. E. Allen, "Modelling dust transport in tokamaks", Europhys. Lett. **83** (2008) 65001.
[84] M. Bacharis , M. Coppins , and J. E. Allen, "Dust in tokamaks: An overview of the physical model of the dust in tokamaks code", Phys. Plasmas **17** (2010) 042505
[85] S. Ratynskaia, L. Vignitchouk, P. Tolias, I. Bykov, H. Bergsåker, A. Litnovsky, N. den Harder and E. Lazzaro, "Migration of tungsten dust in tokamaks: role of dust–wall collisions", Nucl. Fusion **53** (2013) 123002
[86] Y. Tanaka, R. D. Smirnov, A. Yu. Pigarov, H. Takenaga, N. Asakura, Y. Uesugi, N. Ohno, "Simulation of dynamics of carbon dust particles in the JT-60U tokamak", J. Nucl. Mater. **415** (2011) S1106-S1110
[87] T. D. Rognlien, J. L. Milovich, M. E. Rensink, G. D. Porter, "A fully implicit, time dependent 2-D fluid code for modeling tokamak edge plasma", J. Nucl. Mater. **196-198** (1992) 347-351.
[88] S. Wiesen, D. Reiter, V. Kotov, M. Baelmans, W. Dekeyser, A.S. Kukushkin, S.W. Lisgo, R. A. Pitts, V. Rozhansky, G. Saibene, I. Veselova, S. Voskoboynikov, "The new SOLPS-ITER code package", J. Nucl. Mater. **463** (2015) 480-484.